Controlling Pore Size and Wettability of a Unique Microheterogeneous Copolymer Film with Porous Structure

Gang Zhang,† Na Fu,† Hao Zhang,† Jiayu Wang,† Xueliang Hou,† Bai Yang,*,† Jiacong Shen,† Yingshun Li,‡ and Lei Jiang‡

Lab of Supramolecular Structure and Materials, Jilin University, Changchun 130023, China, and Center for Molecular Research, Institute of Chemistry, Chinese Academy of Sciences, Beijing 100080, China

Received March 4, 2002. In Final Form: October 29, 2002

We have fabricated a mesoporous copolymer thin film whose surface pore size can be varied from submicrometer to micrometer. Our fabrication method requires microphase separation induced by a silicone surfactant during the rapid solvent evaporation and polymerizations. The sample films were characterized with atomic force microscopy (AFM), confocal Raman spectroscopy, X-ray photoelectron spectroscopy (XPS), in situ infrared (IR), attenuated total reflection (ATR), and other techniques. The characterization results show that the pore size can be controlled by altering the concentration of silicone surfactant. Furthermore, the mesoporous copolymer film with hydrophobic convex and hydrophilic concave structure exhibits both hydrophobic and oleophobic properties. The unique properties can be attributed to the special heterogeneous porous structure of the polymer film. The resulting porous polymer films can be utilized in many fields, such as self-cleaning, antiadhesives, adsorption, and separation. These mesoscale-patterned surfaces can also provide a model system for investigating the interface properties of actual surfaces.

Introduction

Depending on various fabricated chemical and topological patterns, surface heterogeneities of composition and morphology can dramatically affect interface characteristics.[1] These surface heterogeneities often show a wide variety of interfacial phenomena such as wetting, two-dimensional diffusion, and aggregation. Wettability of solid surfaces is one property that can be manipulated both by varying their chemical composition and by varying their geometrical microstructures.[1−13] Recently, superhydrophobic,[3] superoleophobic,[4] and "amphiphobic" surfaces, which possess both hydrophobic and oleophobic properties,[5] have attracted much interest for their widely practical applications.

Modifying the wetting properties of surfaces by creating well-defined microscopic patterns has attracted increasing scientific and technological attention. To control local surface wettability requires modifying the physical and/or chemical properties of structured surfaces.[6] Various techniques have been developed to produce specifically patterned regions from the micrometer to the nanometer scale with different wettabilities, including micromachining,[7] photolithography,[8] microcontact printing,[9] vapor deposition through grids,[10] Langmuir−Blodgett technique,[11] self-assembled monolayers,[12] and microphase separation in diblock copolymer films.[13] The varied characteristics of the resulting surfaces are of great importance in painting, printing, templating, and even biomedicine, where they make possible selective adhesion and immobilization of cells and biomolecules.

Due to its simplicity, the solvent evaporation method has been an effective way to control the structure of materials.[14] Recently, micropatterned porous materials can be fabricated by self-assembly of block copolymers or by template methods[15−18] during the solvent evaporation

* To whom correspondence may be addressed. Tel: +86-431-8924107. Fax: +86-431-8923907. E-mail: yangbai@jlu.edu.cn.

† Jilin University.

‡ Chinese Academy of Sciences.

(1) (a) Haidara, H.; Mougin, K.; Schultz, J. *Langmuir* **2000**, *16*, 7773. (b) Walheim, S.; Schaffer, E.; Mlynek, J.; Steiner, U. *Science* **1999**, *283*, 520. (c) Wirth, M. J.; Fairbank, R. W. P.; Fatunmbi, H. O. *Science* **1997**, *275*, 44. (d) Roder, H.; Hahn, E.; Brune, H.; Bucher, J. P.; Kern, K. *Nature* **1993**, *366*, 141. (e) Chen, C. S.; Mrksich, M.; Huang, S.; Whitesides, G. M.; Ingber, D. E. *Science* **1997**, *273*, 1425.

(2) (a) Öner, D.; McCarthy, T. J. *Langmuir* **2000**, *16*, 7777. (b) Youngblood, J. P.; McCarthy, T. J. *Macromolecules* **1999**, *32*, 6800.

(3) (a) Nakajima, A.; Fujishima, A.; Hashimoto, K.; Watanabe, T. *Adv. Mater.* **1999**, *11*, 1365. (b) Onda, T.; Shibuichi, S.; Satoh, N.; Tsujii, K. *Langmuir* **1996**, *12*, 2125. (c) Nakajima, A.; Hashimoto, K.; Watanabe, T.; Takai, K.; Yamauchi, G.; Fujishima, A. *Langmuir* **2000,** *16*, 7044. (d) Miwa, M.; Nakajima, A.; Fujishima, A.; Hashimoto, K.; Watanabe, T. *Langmuir* **2000,** *16*, 5754. (e) Barthlott, W.; Neinhuis, C. *Int. Text. Bull.* **2001**, *1*, 9.

(4) Tsujii, T.; Yamamoto, T.; Onda, T.; Shibuichi, S. *Angew. Chem., Int. Ed. Engl.* **1997**, *36*, 1011.

(5) (a) Li, H. J.; Wang, X. B.; Song, Y. L.; Liu, Y. Q.; Li, Q. S.; Jiang, L.; Zhu, D. B. *Angew. Chem., Int. Ed.* **2001**, *40*, 1743. (b) Jiang, L.; Wang, R.; yang, B.; Li, T. J.; Tryk, D. A.; Fujishima, A.; Hashimoto, K.; Zhu, D. B. *Pure Appl. Chem.* **2000**, *72*, 73.

(6) Lenz, P. *Adv. Mater.* **1999**, *11*, 1531.

(7) Abbott, N. L.; Folkers, J. P.; Whitesides, G. M. *Science* **1992**, *257*, 1380.

(8) Wang, R.; Hashimoto, K.; Fujishima, A.; Chikuni, M.; Kojima, E.; Kitamura, A.; Shimohigoshi, M.; Watanabe, T. *Nature* **1997**, *388*, 432; (b) Tadanage, T.; Morinaga, J.; Matsuda, A.; Minami, T. *Chem. Mater.* **2000**, *12*, 590.

(9) (a) Kumar, A.; Whitesides, G. M. *Appl. Phys. Lett.* **1993**, *63*, 2002. (b) Kumar, A.; Biebuyck, H. A.; Whitesides, G. M. *Langmuir* **1994**, *10*, 1498. (c) Xia, Y.; Whitesides, G. M. *Langmuir* **1997**, *13*, 2059. (d) Lopez, G. P.; Biebuyck, H. A.; Frisbie, C. D.; Whitesides, G. M. *Science* **1993**, *260*, 647. (e) Lu, G.; Li, W.; Zhang, G.; Yang, B.; Shen, J. C. *Adv. Mater.* **2002**, *14*, 1049.

(10) Gau, H.; Herminghaus, S.; Lenz, P.; Lipowsky, R. *Science* **1999**, *283*, 46.

(11) (a) Gleiche, M.; Chi, L. F.; Gedig, E.; Fuchs, H. *Chemphyschem* **2001**, *3*, 187. (b) Gleiche, M.; Chi, L. F.; Fuchs, H. *Nature* **2000**, *403*, 173.

(12) Zhang, L.; Zou, B.; Dong, B.; Huo, F. W.; Zhang, X.; Chi, L. F.; Jiang, L. *Chem. Commun.* **2001**, 1906.

(13) Heier, J.; Kramer, E. J.; Walheim, S.; Krausch, G. *Macromolecules* **1997**, *30*, 6610.

(14) (a) Bruinsma, P. J.; Kim, A. Y.; Liu, J.; Baskaran, S. *Chem. Mater.* **1997**, *9*, 2507. (b) Ogawa, M.; Ishikawa, H.; Kikuchi, T. *J. Mater. Chem.* **1998**, *8*, 1783.

10.1021/la025695r CCC: $25.00
Published on Web 02/04/2003

Chart 1. Molecular Structures of the Principal Compounds Used in This Study

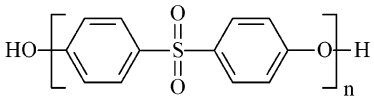

4,4'-dihydroxyl diphenyl sulfone or oligomer (n=1,3,5,7)

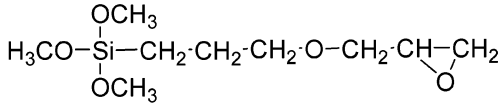

γ-glycidoxy-propyl trimethoxy silane

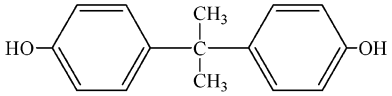

4,4'-dihydroxyl diphenyl isopropane

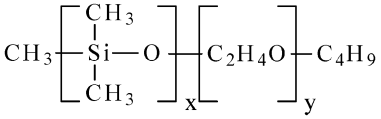

silicone-surfactant

process. But very little has been reported on the properties of the resulting porous materials. Here we report on the preparation of microheterogeneous copolymer film with porous structure through a silicone surfactant induced microphase separation during the rapid solvent evaporation and polymerization process at high temperature. The film was thoroughly characterized by means of atomic force microscopy (AFM), confocal Raman spectroscopy, X-ray photoelectron spectroscopy (XPS), energy-dispersive X-ray analyses (EDX), in situ infrared (IR), and attenuated total reflection (ATR). The results show that the film's surface pore sizes can be widely controlled from the submicrometer to micrometer scale and the film's wettability can be widely adjusted by altering the concentration of silicone surfactant. The resulting unique copolymer film displays both hydrophobic convex and hydrophilic concave structure, which might be responsible for the film's hydrophobic and oleophobic properties. This kind of porous silicone film with unique properties possesses many potential applications, including self-cleaning, antiadhesive properties, adsorption, and separation. Furthermore, the mesoscale-patterned surface can also provide a model system for investigating the interfacial properties of actual surfaces.

Experimental Section

Materials. 4,4′-Dihydroxyl diphenyl sulfone (DHPS), 4,4′-dihydroxyl diphenyl isopropane (DHPP), and dimethyl formamide (DMF) were all obtained from Shanghai Reagent Co. γ-Glycidoxypropyltrimethoxysilane (GPTMS) was purchased from Nanjing Chemical Co. and distilled under reduced pressure before use. Silicone-type surfactant (polydimethylsiloxane oligoethylene oxide block copolymer) was supplied by Shenyang Chemical Co. The oligomers were synthesized by the method previously reported.[19] Some molecular structures of the principal chemical materials used in this study are shown in Chart 1.

Preparation of Sample Film. The prepared oligomer (n = 5) was dissolved into dimethylformamide (DMF), before γ-glycidoxypropyltrimethoxysilane was added to the solution. 4,4′-Dihydroxyl diphenyl isopropane was used for contrasting spectroscopy experiments and replacing 4,4′-dihydroxyl diphenyl sulfone or its oligomer. The mass ratio of oligomer:GPTMS:DMF was about 1.0:0.4:9.0. Different proportions of silicone-type surfactant (polydimethylsiloxane oligoethylene oxide block copolymer) were added to the solution for further experiment. The mixed solution requires stirring more than 12 h to make it homogeneous prior to use.

Before we used them as substrates, we cleaned the silicon wafers according to the following procedures: (i) treatment for 2 h with a solution of 70% H_2SO_4/30% H_2O_2 at 80 °C; (ii) washing in water; (iii) rinsing with deionized water thoroughly; and finally (iv) drying in a nitrogen flow.

The silicon wafers were immersed in the coating solution for 3 min, and the speeds of immersion and extraction were controlled at 1 mm/s. The coating was heated to cure at 210 °C for 15 min. In addition, we conducted experiments at different temperatures: 25, 75, 125, 150, and 175 °C, to compare the resulting effects. A few samples were heated directly in the hot stage on the optical microscope for an in situ observation.

Characterization. Fourier transform infrared (FT-IR) spectrometer (Nicolet Instrument Corporation, Avatar 360) was adopted to investigate the process of solvent evaporation and curing reaction, using the standard KBr pellet method. Multi-Bounce HATR accessory was used to detect attenuated total reflection (ATR) spectra. X-ray photoelectron spectroscopy (XPS) was performed on a VG ESCALAB MK II spectrometer, using a monochromatic Mg Kα X-ray source operated at 300 W and 10^{-7} Pa vacuum degree.

Confocal Raman spectra were obtained with a Renishaw Raman imaging microscope system 1000 spectrometer equipped with a Ge detector. The spectral resolution was 4 cm^{-1}, and the laser power at the sample point was kept below 50 mW for the films.

Atomic force microscopy (AFM) observations of the film surfaces were carried out with a commercial instrument (Digital Instrument, Nanoscope IIIa, Multimode), under ambient conditions at room temperature. AFM height images and lateral force microscopy (LFM) friction images were simultaneously recorded on contact mode AFM. Triangular Si_3N_4 cantilevers with pyramidal tips purchased from Nanosensor were used. All tapping mode images were measured at room temperature in air with the microfabricated rectangle crystal silicon cantilevers (Nanosensor). Topography and phase images were obtained simultaneously using a resonance frequency of approximate 365 kHz for the probe oscillation. For most of our investigations, we adopted a set point at 0.9−1.3 V. Scanning electron microscopy (SEM) images were collected on a JEOL JAX-840 electron microscope. Energy-dispersive X-ray analyses (EDX) were recorded on SEM OXFORD ISIS-300 EDS accessory (U.K.). The process of forming film was observed using an optical microscope in reflection mode (XSP-BM) fitted with a Panasonic color charge-coupled device (CCD) video camera and a heating stage (200 W).

The contact angles were measured by a contact angle meter (Drop Shape Analysis System DSA20 MK2 KRÜSS Edward Keller Ltd) at a temperature of 23 ± 1 °C and humidity of 30 ± 5%. Pure water and n-hexadecane were used for the contact angle measurements. The amount of one liquid droplet was about 4 μL.

Results and Discussion

Morphology and Properties of the Film Surface. Figure 1 displays the AFM topography and LFM images

(15) (a) Templin, M.; Franck, A.; Du Chesne, A.; Leist, A.; Zhang, A.; Ulrich, R.; Schädler, V.; Wiesner, U. *Science* **1997**, *278*, 1795. (b) Zhao, D.; Feng, J.; Huo, Q.; Melosh, N.; Fredrickson, G. H.; Chmelka, B. F.; Stucky, G. D. *Science* **1998**, *279*, 548.

(16) (a) Velev, O. D.; Jede, T. A.; Lobo, R. F.; Lenhoff, A. M. *Nature* **1997**, *389*, 447. (b) Holland, B. T.; Blanford, C. F.; Stein, A. *Science* **1998**, *281*, 538. (c) Matsushita, S.; Miwa, T.; Fujishima, A. *Chem. Lett.* **1997**, 925.

(17) (a) Imhof, A.; Pine, D. J.; *Adv. Mater.* **1998**, *10*, 697. (b) Karthaus, O.; Maruyama, N.; Cieren, X.; Shimomura, Hasegawa, M. H.; Hashimoto, T. *Langmuir* **2000**, *16*, 6071. (c) Nishikawa, T.; Nishida, J.; Ookura, R.; Nishimura, S.; Scheumann, V.; Zizlsperger, M.; Lawall, R.; Knoll, W.; Shimomura, M. *Langmuir* **2000,** *16*, 1337.

(18) (a) Widawski, G.; Rawiso, B.; Francüois, B. *Nature* **1994**, *369*, 387. (b) Francüois, B.; Pitois, O.; Francüois, J. *Adv. Mater.* **1995**, *7*, 1041. (c) Jenekhe, S. A.; Chen, X. L. *Science* **1999**, *283*, 372.

(19) Yang, Y.; Li, Y.; Shen, J. *Chem. J. Chin. Univ.* **1989**, *10*, 276.

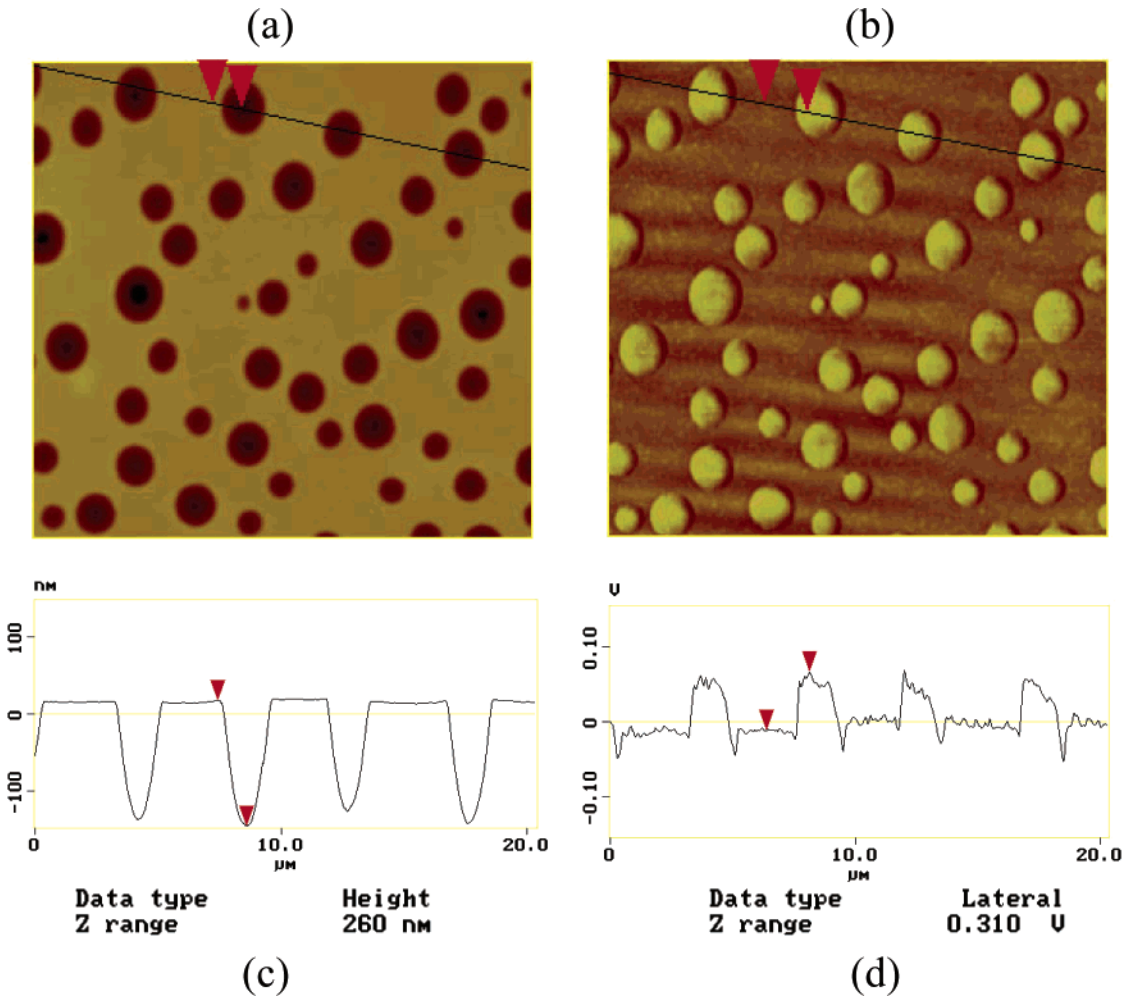

Figure 1. Contact mode AFM images of film surface prepared from 1.50% surfactant coating solution and cured at 200 °C: (a) height image (20 μm × 20 μm); (b) lateral force image; (c) cross-sectional profile of (a); (d) cross-sectional profile of (b).

of a cured film, which was prepared from the solution containing 1.5% surfactant. Micrometer-size pores are observed in the topographic image (Figure 1a), with a pore density of about $10^7/cm^2$. While the LFM image of the same area shows that the frictional properties inside and outside of the pores are quite different (Figure 1b), all lateral forces (frictional forces) on the surface inside of the pores were consistently larger than those on the outside surface at the same load. Without considering the scanning effects such as edge effect, the contrast in the LFM image can be attributed to the fact that the uncoated hydrophilic Si_3N_4 tip may generate a stronger friction force at the hydrophilic area than at the hydrophobic area.[5b,20,21] In the cross sections of topography and LFM images (Figure 1c,d), we can observe that the lower regions on the surface correspond to the regions with higher surface friction (about 3 times higher than low friction[20,22]). The above results indicate that there are more functional groups with high surface free energies on the inner wall of the pores than those on the outer surface, suggesting that the component with lower surface energy is enriched on the flat surface.

In the tapping mode AFM topography and phase images of the same sample (Figure 2), pores and surrounding matrix are observed both in topography and phase images. Different from the topography image, the surrounding matrix has the same dark color in the phase image, while all the pores are a relatively uniform bright color. Apparently, the contrast observed in the phase image is not significantly influenced by topography variations from the above images. Considering that all experiments were carried out under the same conditions, this contrast suggested that the brighter color areas be related to the domains of the softer (low Young's modulus) or high adhesion components; on the contrary, the darker color areas correspond to the harder (high Young's modulus) or low adhesion components.[20,23] It is clear that the viscoelasticities on the inner wall of the pores and on the surrounding matrix surface are quite different. Obviously, different surface properties correspond to different terminal groups on the topmost few angstroms at the surface.[24] These conclusions are in good agreement with the contact mode AFM results.

(20) Takano, H.; Kenseth, J. R.; Wong, S. S.; O'Brien, J. C.; Porter, M. D. *Chem. Rev.* **1999**, *99*, 2845.
(21) (a) Green, J. B. D.; McDermott, M. T.; Porter, M. D.; Siperko, L. M. *J. Phys. Chem.* **1995**, *99*, 10960. (b) Kendall, K. *Nature* **1986**, *319*, 203.
(22) (a) Lio, A.; Charych, D. H.; Salmeron, M. *J. Phys. Chem. B* **1997**, *101*, 3800. (b) Overney, R. M.; Meyer, E.; Frommer, J.; Guntherodt, H. J.; Fujihjira, M.; Takano, H.; Gotoh, Y. *Langmuir* **1994**, *10*, 1281.
(23) (a) Leclere, P.; Lazzaroni, R.; Bredas, J. L.; Yu, J. M.; Dubois, P.; Jerome, R. *Langmuir* **1996**, *12*, 4317. (b) Tamayo, J.; Garcia, R. *Langmuir* **1996**, *12*, 4430. (c) Raghavan, D.; Vanlandingham, M.; Gu, X.; Nguyen, T. *Langmuir* **2000**, *16*, 9448.
(24) (a) Finot, M. O.; McDermott, M. T. *J. Am. Chem. Soc.* **1997**, *119*, 8564. (b) Whangbo, M. H.; Bar, G.; Brandsch, R. *Surf. Sci.* **1998**, *411*, 794. (c) Tamayo, J.; Garcia, R. *Langmuir* **1996**, *12*, 4430. (d) Anezykowski, B.; Kruger, D.; Fuchs, H. *Phys. Rev. B* **1996**, *53*, 15485.

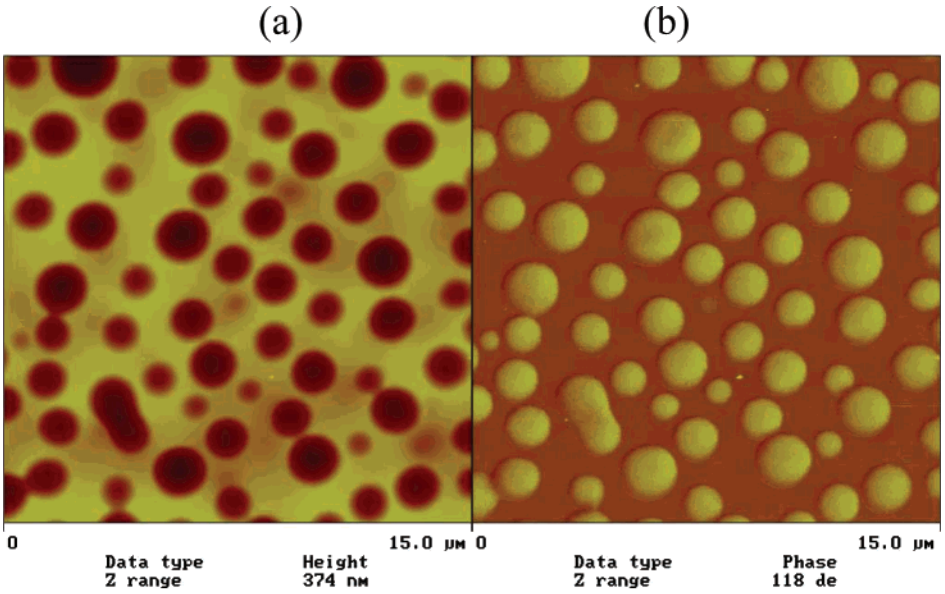

Figure 2. Tapping mode AFM images of film surface: (a) height image; (b) phase image. The brighter domains have more phase shift than the darker domains.

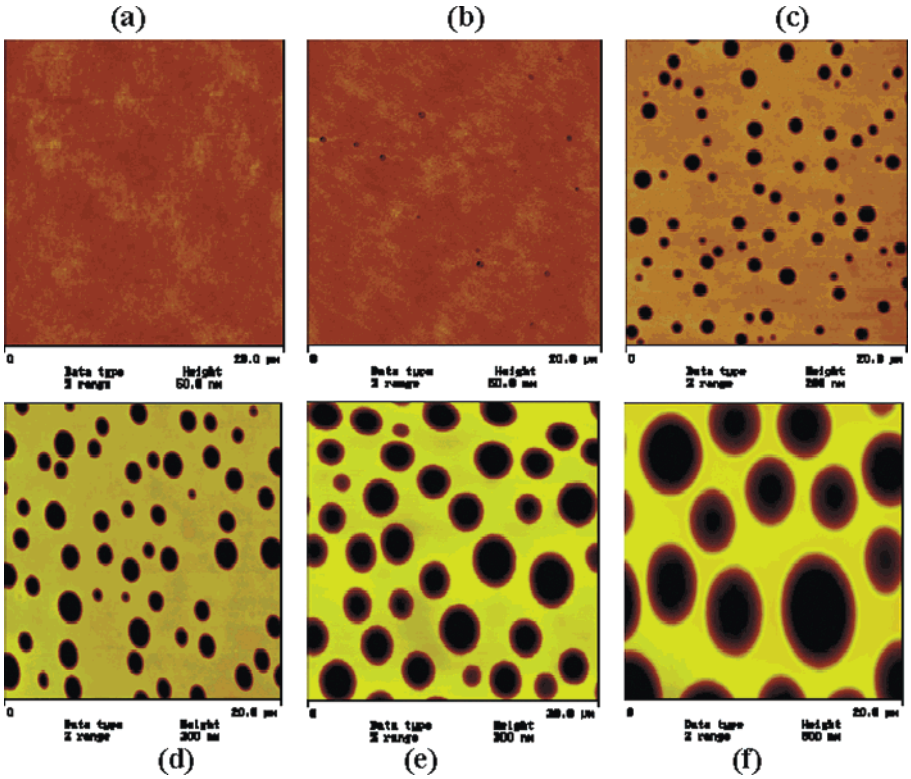

Figure 3. AFM topography images of film surfaces prepared from solutions containing surfactant: (a) 0%; (b) 0.05%; (c) 0.5%; (d) 1.5%; (e) 3.0%; (f) 6.0%.

Figure 3 gives six AFM topography images of film surfaces prepared from solutions containing 0−6.0% surfactant. When there was no surfactant in the solution, the cured film was flat and poreless (see Figure 3a), so the surface roughness was very low and the root-mean-square (rms) value was 0.478 nm (shown in Table 1). After a small amount of surfactant (0.05%) was added to the solution, some small pores appeared on the cured film (Figure 3b), and the rms value increases to 0.555 nm. As the surfactant concentrations increase from 0.5 to 6.0%, we can observe more and larger pores on the cured films (see Figure 3c−f). Table 1 gives us the diameters, depths, fractions of pores, and rms roughness in detail. The diameters of the pores varied from 0.27 to 3.52 μm, and the depths of the pores lengthened from 28.2 to 326.7 nm. Correspondingly, the rms roughness increased from 0.478 to 100.054 nm. Furthermore, the surface fractions of the pores on the flat (f_p) changed from 3.7% to 83.5% and the pore densities were in the range of 10^6−10^7/cm^2. The above results indicate that the surfactant is a critical factor in the process of pore formation. Apparently, it can decide whether the pores can form or not, and affect the pore size. The more surfactant added in the preparation process, the more pores would form on the surface, and the bigger the fraction of surface containing pores would grow.

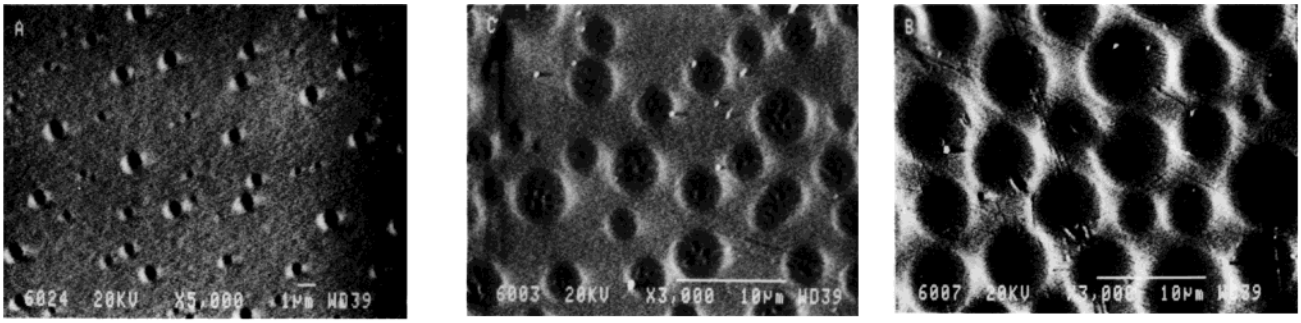

(a) (b) (c)

Figure 4. SEM images of film surfaces prepared from solutions containing surfactant: (a) 0.5%; (b) 1.5%; (c) 3.0%.

Table 1. Statistics Data Describing Diverse Surface Topography and Wetting Properties[a]

% surfactant	pore diameter (μm)	pore depth (nm)	% pore fraction	rms roughness (nm)	θ_{H_2O} (deg)	θ_{oil} (deg)
0	0	0	0	0.478	60.5	16.4
0.05	0.27	28.2	3.7	0.555	89.2	31.5
0.25	0.68	48.4	7.1	7.652	92.3	31.3
0.50	1.07	91.5	13.4	20.811	96.0	32.2
0.75	1.47	109.8	22.4	20.491	96.7	31.6
1.00	1.54	139.6	24.4	34.539	99.4	34.2
1.50	1.90	155.3	29.7	37.254	102.4	33.5
2.00	2.24	161.3	35.1	49.320	105.8	35.5
3.00	2.64	167.2	50.8	52.604	108.2	36.2
5.00	2.90	219.3	63.9	74.972	113.5	36.3
6.00	3.52	326.7	83.5	100.054	126.3	38.5
1.50[b]				37.827	54.4	
1.50[c]				1.509	52.5	

[a] Diameter and height data from average value. rms (root mean square) roughness data from AFM image statistics. θ_{H_2O} and θ_{oil} are the equilibrium contact angles for water and *n*-hexadecane. All film was cured at 210 °C for 15 min except where noted. [b] All film was cured at 25 °C for 10 days;. [c] All film was cured at 75 °C for 5 h.

Evidently, we can control the pore size on the cured film by changing the concentration of the surfactant.

The SEM images of three cured films prepared from solutions containing 0.5%, 1.5%, and 3.0% surfactant, respectively, are shown in Figure 4. It is easy to see that as pores distribute on the surface of the three cured films, their diameters grow from submicrometer to several micrometers in size. These results further confirmed our AFM measurements.

Analysis of the Cure Process by in Situ IR Spectroscopy. The process of solvent evaporation and curing was characterized by in situ IR spectroscopy. Figure 5 shows the in situ IR spectra recorded at different temperatures during the process of heating. The IR spectrum of DMF shows the characteristic bands at 1695−1615 cm^{-1} (carbonyl group absorption) and the band at near 1400 cm^{-1} (C−N absorption). From line a to line h, the bands at 1695−1615 and 1400 cm^{-1} became weaker and gradually vanished as the temperature increased from 25 to 220 °C. These spectrum changes correspond to the evaporation process of solvent, indicating that the solvent begins to evaporate at 125 °C and finishes at near 210 °C.

The characteristic absorption band of phenolic O−H stretch vibration appears at 3140 cm^{-1} (Figure 5a). At room temperature, this band generally appears at the region of 3200−3500 cm^{-1} due to the effect of hydrogen bonding. When the temperature rose from 25 to 125 °C, the band red shifted from 3140 to 3300 cm^{-1} (Figure 5b−d). When the temperature reached 150 °C, the band shifted to 3360 cm^{-1} and achieved its strongest intensity (Figure 5e). As the temperature rose further from 150 to 220 °C, the band started to blue shift and became weaker. Such changes of in situ IR spectra can be explained as follows: (i) when the temperature is below 150 °C, the band red shifts because the "electron attraction effect" of sulfone ($-SO_2-$) in the sulfonyldiphenol molecule is very strong. Furthermore, under the strong "electron attraction effect", the combining of phenolic O−H with the N of DMF to form hydrogen bonding occurs more easily. (ii) When the temperature reaches the boiling point of solvent DMF, phenolic hydroxyl is liberated from its hydrogen bonds along with the rapid evaporation of DMF. This transition can be observed in the change of the characteristic NH^+ absorption band, which appears at the region of 2700−2600 cm^{-1}. When the temperature is below 150 °C, the band usually gives two clear small peaks (Figure 5a−f); when the temperature is above 150 °C, the two peaks weaken and disappear completely (Figure 5g−i).

For epoxy groups in GPTMS, the band of three-membered epoxide ring C−O stretch vibration appears at 1240 cm^{-1}, which is different from the bands of sulfonyldiphenol's Ph−O that appear at 1284 and 1224 cm^{-1} (see Figure 5a−d). Below 125 °C, the ring skeletal vibration near 909 cm^{-1} is clear, but the band becomes weaker as the temperature increases from 20 to 125 °C and finally vanishes at 150 °C (Figure 5e). This change indicates that the epoxy groups of the solution begin to react at 125 °C and finish reacting at about 150 °C.

While the characteristic epoxy group absorption band vanishes at 150 °C, a new band appears at near 930 cm^{-1} (Figure 5e), which can be attributed to the vibration of the Si−O−Ph group originating from the reaction between Si−O−CH_3 and Ph−OH. The characteristic absorption band of Si−O−CH_3 (at about 1090 cm^{-1}) begins to decrease at 125 °C (Figure 5d) and reaches equilibrium at 210 °C (Figure 5h). In the IR spectrum, both S−Ph and Si−O−CH_3 vibrations often appear at near 1090 cm^{-1}, so it is difficult for us to pinpoint the changed of Si−O−CH_3 vibration. Because 4,4′-isopropylidenediphenol not only has a similar molecular structure to 4,4′-sulfonyldiphenol but also possesses no S−Ph group, it can be used to distinguish the vibrations of S−Ph and Si−O−CH_3 groups. We found that those contrasting spectra (4,4′-sulfonyldiphenol was replaced by 4,4′-isopropylidenediphenol) are very similar to those in Figure 5, except we found no little peak at 1070 cm^{-1} (the spectra are not included here). We conclude that the band changes are mainly attributable to the Si−O−CH_3 group, suggesting that the Si−O−CH_3 and Ph−OH begin to react at 125 °C and reach equilibrium at 210 °C.

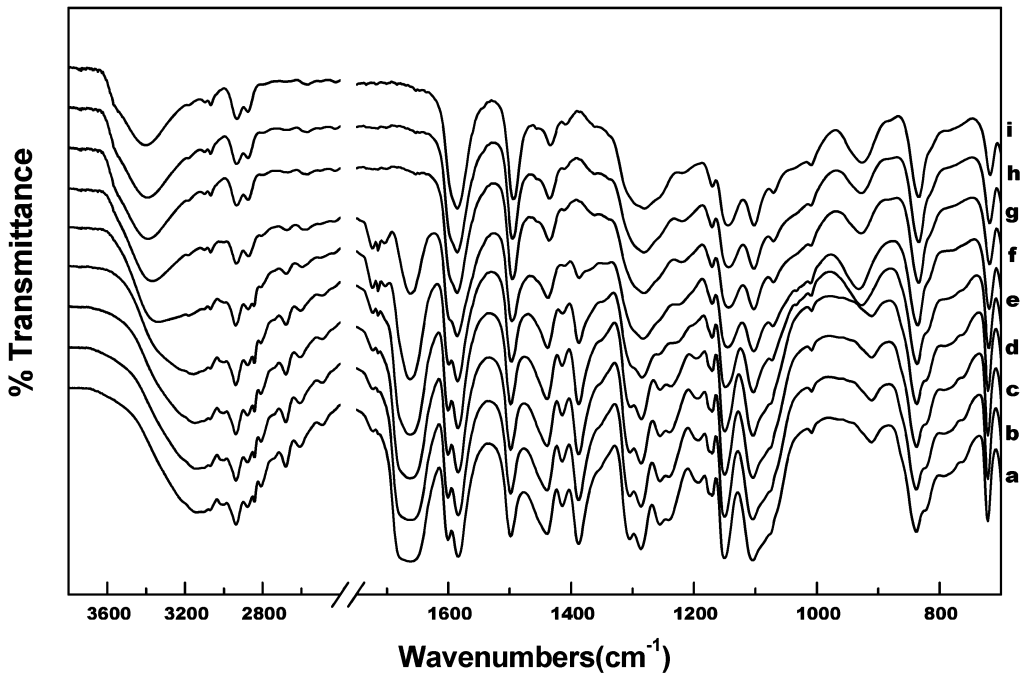

Figure 5. In situ FTIR spectra recorded at (a) 20 °C; (b) 50 °C; (c) 100 °C; (d) 125 °C; (e) 150 °C; (f) 175 °C; (g) 200 °C; (h) 210 °C; (i) at 220 °C for 10 min.

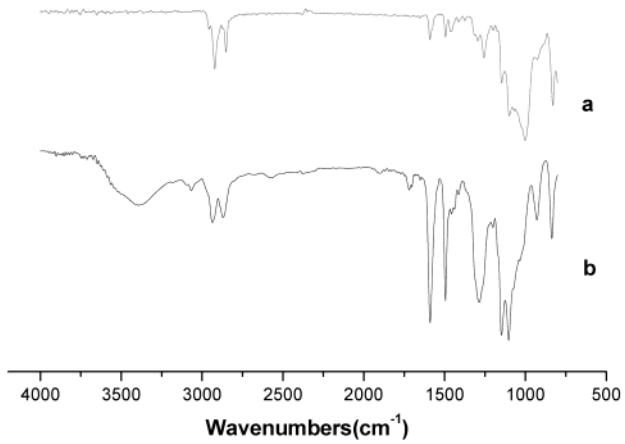

Figure 6. (a) The FTIR spectrum of the film and (b) the ATR spectrum of film surface.

Our analyses led us to suggest that two chemical reactions occur in our solution:

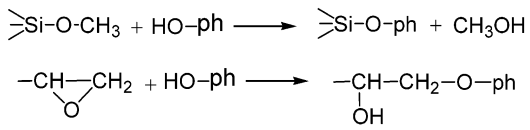

Both reactions start rapidly at the beginning of solvent evaporation (125−150 °C) and reach equilibrium at 210 °C, just when the solvent finishes evaporating.

Analysis of the Groups on the Surface. *IR and ATR.* Both the IR spectrum of the film and ATR spectrum of the film surface were measured for further detection of the chemical composition and distribution on the film surface (shown in Figure 6). The IR spectrum of the film (Figure 6a) is similar to the ATR spectrum of the film surface (Figure 6b) although the band intensity for the film surface is a little weaker. Such an observation implies that most functional groups, such as methyl and methylene (2948−2841 cm^{-1}), benzene (1650−1443 cm^{-1}), sulfone (1100 cm^{-1}), and Si−O−R (1090−1100 cm^{-1}), exist both in the film and on the surface of the cured film. Furthermore, the hydroxyl stretch vibration band (3400−3300 cm^{-1}) can be seen in the IR spectrum of film but it cannot be found on the film surface in the ATR detection region (micrometer scale), suggesting that fewer functional groups with high surface free energies (such as hydroxyl) distribute on the surface of film rather than those with low surface free energies. This distinction can be further proved by the following results of XPS and EDX.

Table 2. The Atomic Percentage of Different Elements Collected from XPS and EDX Analysis Data

conditions	C (wt %)	O (wt %)	Si (wt %)	S (wt %)
a	64.46	24.74	7.80	2.99
b	66.70	21.36	9.52	2.43
c	50.42	23.64	25.07	0.87
d	51.59	23.22	24.08	0.81
e	62.01	28.19	5.71	4.09

[a] Without silicone surfactants and cured at 210 °C for 10 min detected by XPS. [b] Contains 1.5% silicone surfactants and cured at 25 °C, detected by XPS. [c] Contains 1.5% silicone surfactants and cured at 210 °C for 10 min detected by XPS. [d] Contains 1.5% silicone surfactants and cured at 210 °C for 10 min, after which was stored for 50 days, detected by XPS. [e] Contains 1.5% silicone surfactants and cured at 210 °C for 10 min detected by EDX.

XPS and EDX. XPS and EDX analyses can give us chemical information about various elements on the film surface from several nanometers to micrometer thickness. The atomic percentages of four elements collected from EDX and XPS detections are summarized in Table 2. When there is no surfactant in the coating solution (cured at 210 °C, line A) or the coating solution is prepared from 1.5% silicon-surfactant (cured at 25 °C, line B), the content of Si is relatively low (detected by XPS). When the curing temperature reaches 210 °C (1.5% silicon surfactant in the coating solution), the percentage of Si increases about three times (line C) compared with film cured at 25 °C and remains at the same value for more than 50 days (line D). In contrast, EDX analyses give the lowest value of the film surface (line E) under the same treatment, because the detection depth of EDX (∼1 μm) is much deeper

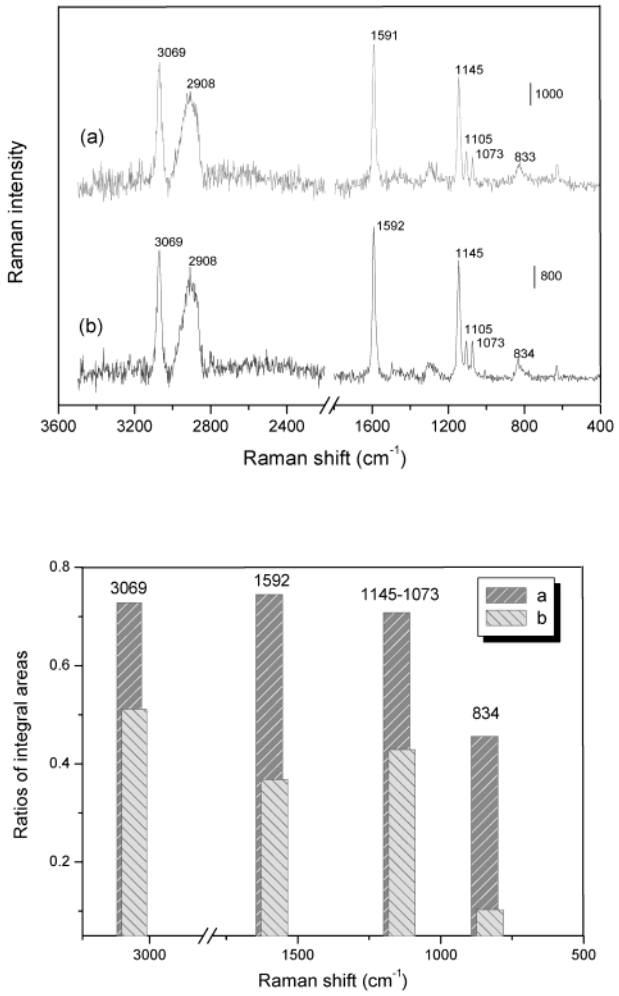

Figure 7. (top) Confocal Raman spectra of film surface: (a) inner wall of the pore and (b) surrounding matrix. (bottom) Integral area of Raman bands to integral area of the band centered at 2908 cm^{-1} ratios: (a) inner wall of the pore and (b) surrounding matrix.

than that of XPS (4−10 nm). Generally, silicon groups (such as Si−O−R and Si−O−Si) have low surface free energies and the surface free energies will decrease when the percentage of Si increases. We concluded that rapid solvent evaporation and curing at a high temperature could both induce the functional groups with low surface free energies to accumulate on the surface of the film and induce the functional groups with high surface free energies (such as hydroxyl) to accumulate deep within the film at the same time. In other words, more and more functional groups concentrate on the interface between film and air than on the deeper layer (>10 nm) of the film.

Confocal Raman Spectroscopy. The advent of confocal Raman spectroscopy has opened a new way to detect chemical information on the microscopic scale. Because the confocal laser can be focused on a single pore, chemical information about the pores' inner walls and their surrounding matrix surface can be obtained. Figure 7 shows the comparison of the confocal Raman spectrum of the inner wall of a pore (curve a) and surrounding matrix (curve b). Both Raman spectra give seven typical bands at 3069, 2098, 1591, 1145, 1105, 1073, and 834 cm^{-1}. The band at 3069 cm^{-1} is attributable to the aromatic C−H stretching vibration of sulfonyldiphenol units, and the bands at 2917−2879 cm^{-1} are assigned to the C−H stretching vibrations of methyl and methylene in the alkyl

Scheme 1. Proposed Route of the Rapid Solvent Evaporation and Cure Process

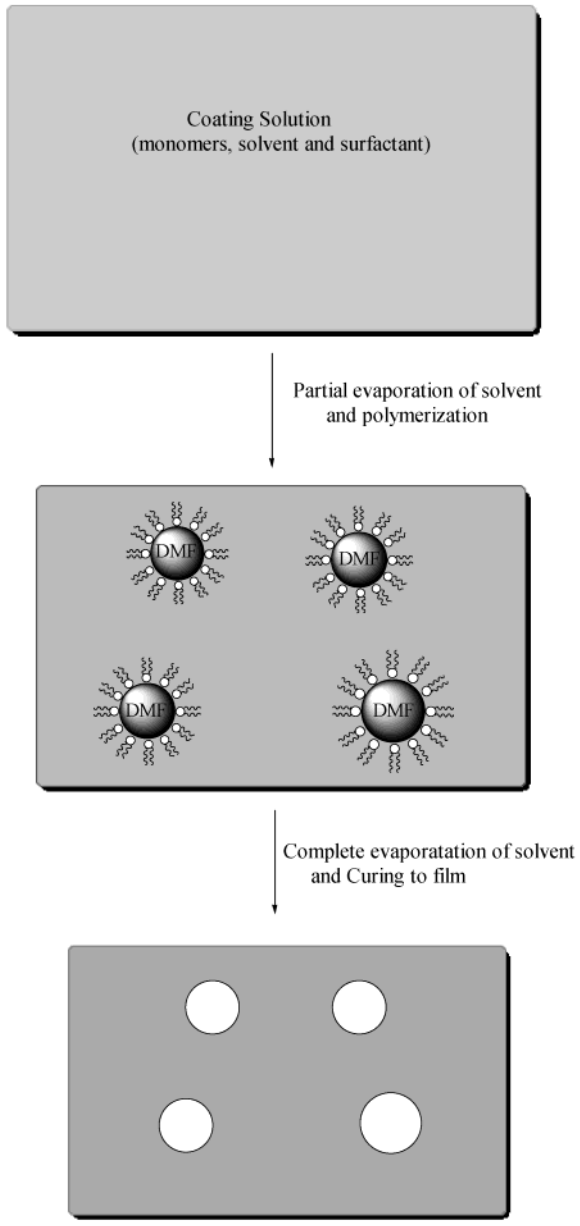

chain. Two bands at 1591 and 1145 cm^{-1} can be attributed to the ring stretching vibration of benzene and the symmetric stretching mode of sulfonyl, respectively. The bands of the aromatic C−S vibration of sulfonyldiphenol often appear at 1105 and 1073 cm^{-1}. The broad band centered at 833 cm^{-1} can be ascribed to the symmetric stretching vibration of the C−O−C bond with some contribution from 1,4-disubstituted phenyl. From the Raman spectra and the corresponding column graph, we find that the integral areas of the bands at 3069, 1591, 1145, 1105, 1073, and 833 cm^{-1} compared to the integral area of the broad band centered at 2908 cm^{-1} ratios obtained in Raman spectrum a are much larger than those ratios obtained in spectrum b. These bands are associated with the vibrations of sulfonyldiphenol and ether units, which show more polarity than aliphatic chains in the polymer. We infer that there are more polar units of sulfone ($-SO_2-$) and ether (C−O−C) on the inner wall of the pores than on the surrounding matrix surface. Contact mode AFM and tapping mode AFM results are also consistent with the above suggestions.

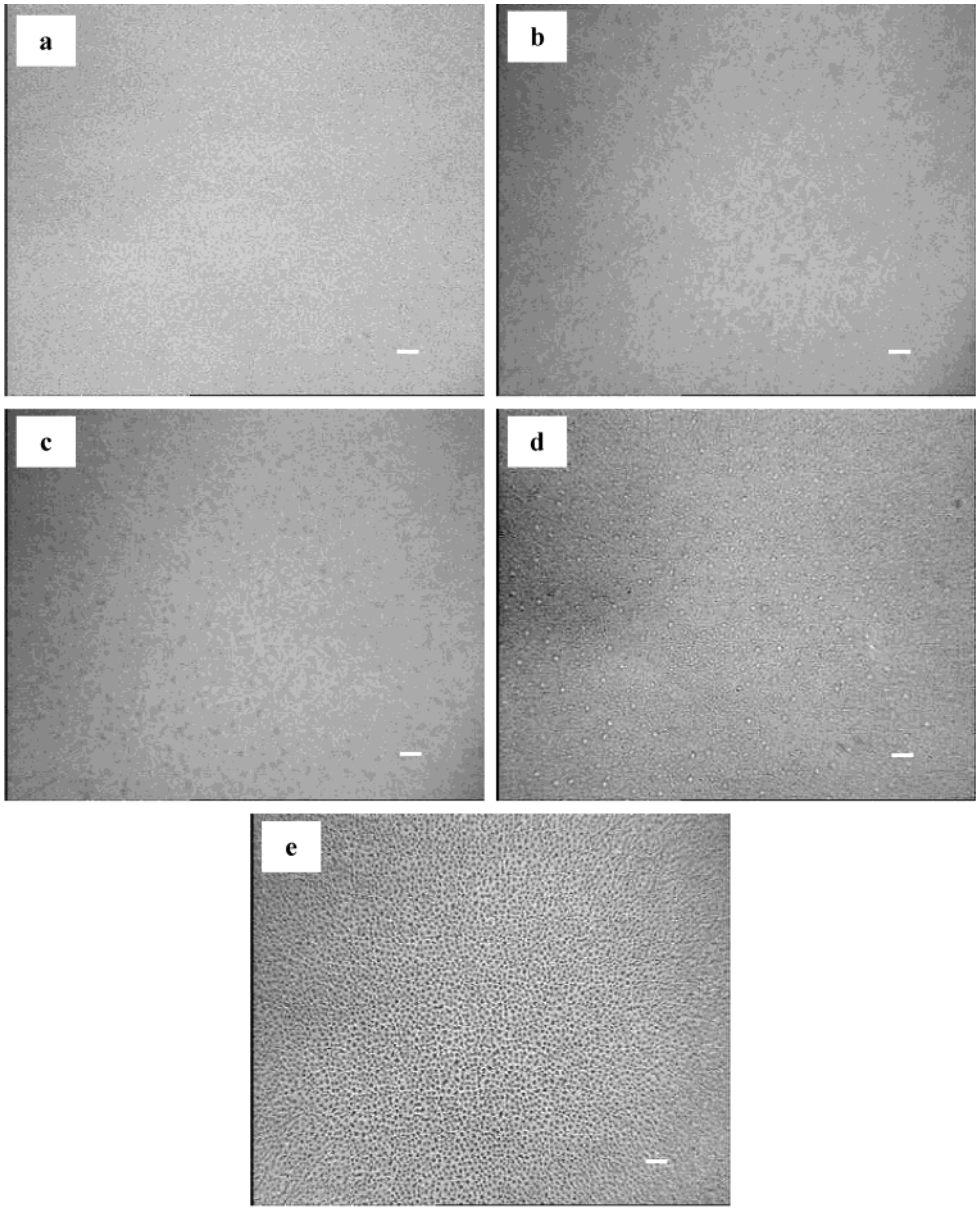

Figure 8. In situ optical micrographs of the curing process taken after (a) 0, (b) 235, (c) 240, (d) 245, and (e) 270 s total annealing time at 200 °C. The bar in each case represents 15 μm.

We propose the following mechanism: At first, as the temperature rose, the solvent gradually evaporated. Simultaneously, the surfactant-induced functional groups and segments of polymerizing chain with high surface free energies assembled while the decreasing spherical solvent formed large "reverse micelles" in this process. Then, after the solvent completely evaporated (boiling away), the functional groups with high surface free energies remained on the bubbling inner walls. At the same time, the surface shape solidified by complete cross-linking polymerization. Scheme 1 describes this mechanism. We think that the droplet number increased with surfactant concentration, then more droplets with high density formed larger droplets, so their size increased with surfactant concentration. We can observe this trend from the AFM and SEM images.

In situ optical microscopy images (Figure 8) depict the forming film process: The solution (1.5% surfactant) on the surface is a homogeneous phase (a), when it was heated the solvent evaporated gradually. After 235 s, solvent droplets, as emulsion colloid (large "reverse micelles") formed (the black points in (b), but they were mobile (from b to c and d). After 270 s, the surface was solidified, the solvent droplets boiling away, and pores formed on the surface just as shown in image e. These observations support our proposed mechanism for the process of forming film with porous structure.

The Effect of Process Temperature. Curing temperature often plays an important role in the process of the film formation, so we examined the AFM topography 3D images of the cured films at various curing temperatures. From the three images of Figure 9, we can see that the surfaces exhibit different morphology and roughness at different temperatures. In Figure 9a there is apparently no pore in the film cured at 25 °C, but there are disorder phase separate domains. When the curing temperature increased to 75 °C, the film surface still showed no pore (Figure 9b). At 150 °C, pores began to appear on the film surface, but their shapes were not clear (Figure 9c). At 210 °C, many uniform pores appeared at the film surface (Figure 9d). From this progression, we conclude that the forming of pores requires rapid evaporation of the solvent. The high curing temperature is evidently necessary. Coordination between the solvent

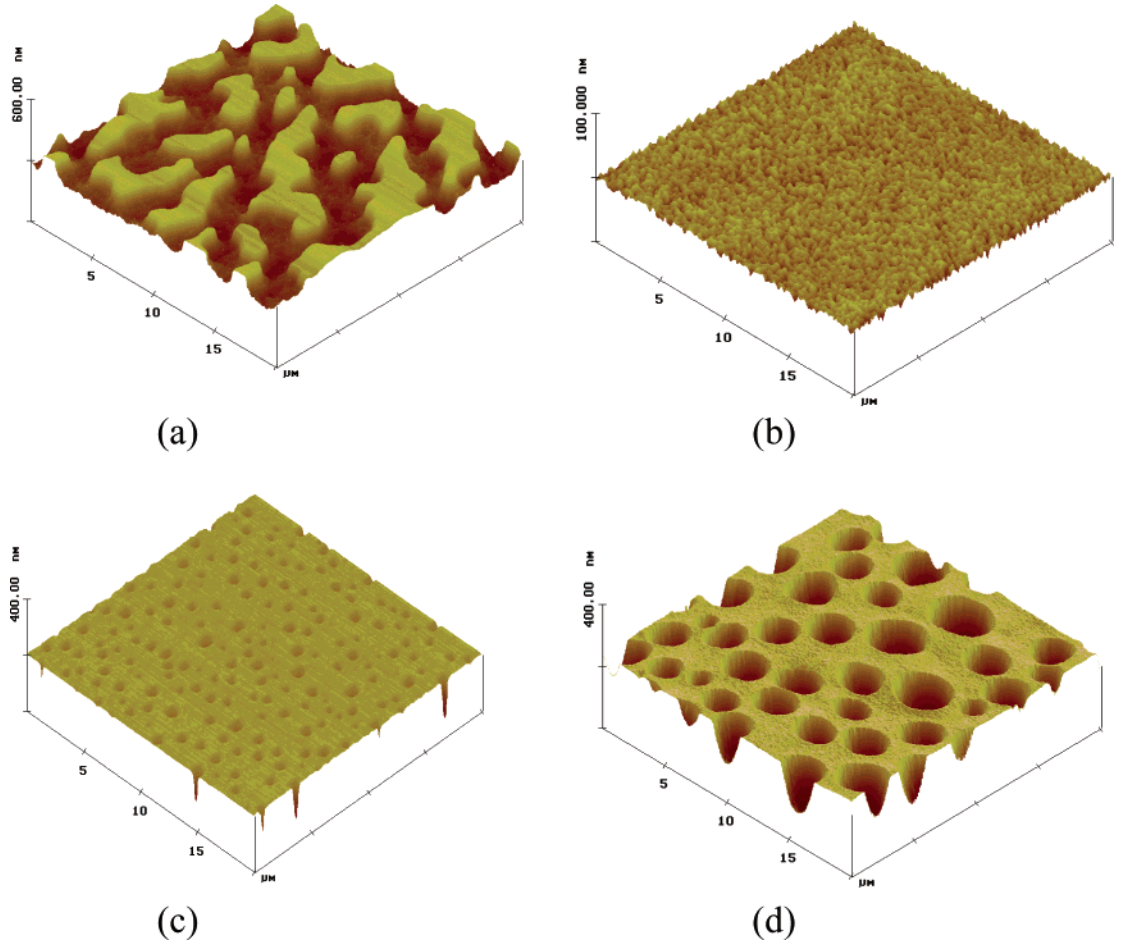

Figure 9. AFM 3D images of the cured films at various curing temperatures: (a) 25 °C; (b) 75 °C; (c) 150 °C; (d) 210 °C.

evaporation speed and the film curing (polymerization) speed is very important. Their matching can decide whether the pores form. When curing temperature reaches 210 °C, both speeds can be controlled very well.

Wettability of the Film. Interestingly, porous copolymer film surfaces show unique dewetting properties for both water and oil. When there is no surfactant, the cured film surface remains flat, the contact angles are 60.5° for water and 16.4° for oil (see Table 1). When the number of surface pores increases, contact angles for both water and oil increase. When the surfactant varies from 0 to 6.0%, pore fraction increases from 0 to 83.5%, the rms roughness increases from 0.478 to 100.05 nm, the contact angle for pure water increases from 60.5° to 126.3°, and the contact angle for oil increases from 16.4° to 38.5°. Apparently, for the structured film, the contact angles both for water and for oil increase simultaneously.

We noted that films containing surfactant but cured at relatively low temperatures (such as 25 and 75 °C) show poreless structure and contact angles similar to that of the planar surface with no surfactant. Apparently, the hydrophobic property of the film is not caused by the hydrophilic surfactant itself, while porous structure is more important.

Contact angle Cassie[25] and Wenzel equations[26] give two laws valid for smooth but chemically heterogeneous substrates and rough but chemically homogeneous surfaces, respectively. There are many references in the literature for the modification of these laws.[27,28] Our experimental results lead us to conclude that the distribution of functional groups on the new material surface dramatically changed induced by silicone surfactant. Distribution of domains, polarity of pores, and nonpolarity of the surface (hydrophilic and hydrophobic properties) were totally different from the homogeneous flat surface. Induced by the surfactant, more polar groups aggregated on the wall of pores and more hydrophobic groups distributed on the surface of film. The wetting properties of this porous surface are completely different from those of a general homogeneous planar surface, which could be reasonably attributed to the unique film structure.

Conclusion

We prepared mesoporous copolymer film through a silicone surfactant induced spontaneous microphase separation during the process of rapid solvent evaporation and polymerization. By altering the concentration of silicone surfactant, we varied the pore size from submicrometer to micrometer size. The characterization results of IR,

(25) (a) Cassie, A. B. D. *Discuss. Faraday Soc.* **1948**, *3*, 11. (b) Drelich, J.; Miller, J. D. *Langmuir* **1993**, *9*, 619. (c) Woodward, J. T.; Gwin, H.; Schwartz, D. K. *Langmuir* **2000**, *16*, 2957. (d) Urban, D.; Topolski, K.; Coninck, D. *J. Phys. Rev. Lett.* **1996**, *76*, 4388.

(26) (a) Wenzel, R. N. *J. Phys. Colloid Chem.* **1949**, *53*, 1466. (b) Borgs, C.; Coninck, J. D.; Kotecky, R.; Zinque, M. *Phys. Rev. Lett.* **1995**, *74*, 2292. (c) Miller, J. D.; Veeramasuneni, S.; Drelich, J.; Yalamanchili, M. R. *Polym. Eng. Sci.* **1996**, *36*, 1849. (d) Swain, P. S.; Parry, A. O. *Eur. Phys. J., B* **1998**, *4*, 459.

(27) (a) Drelich, J. J. *Colloids Surf., A* **1996**, *116*, 43. (b) Drelich, J.; Miller, J. D. *Langmuir* **1993**, *9*, 619. (c) Toshev, B. V.; Platikanov, D.; Scheludko, A. *Langmuir* **1988**, *4*, 489.

(28) Tröger, J.; Lunkwietz, K.; Bürger, W. *J. Colloid Interface Sci.* **1997**, *194*, 281.

ATR, XPS, and EDX indicate that there are more Si−O groups and fewer hydroxyl groups on the film surface than in the deeper layer of the film. The resulting mesoporous copolymer film with hydrophobic convex and hydrophilic concave structure displays both hydrophobic and oleophobic properties, which can be widely varied by altering the surfactant. This unique controlled wettability originates from the special heterogeneous porous structure of the polymer film. Distributions of microheterogeneous domains, and surface roughness are the main reasons for dewetting, not only for water but also for oil.

Acknowledgment. This work was supported by NSFC (No.29925412, 50073007) and the Major State Basic Research Development Program (G2000078102). The authors thank Dr. Barbara Whitesides for her correction on the writing of this paper.

LA025695R